

MAGNET BEAM ABSORBERS  
of the  
350 GeV/c Dichromatic Train

S.Mori and H.STREDDE

January 24, 1978

I. Introduction

The schematic diagram of the 350 GeV/c Dichromatic Train (N-30)<sup>1</sup> which is presently under construction is shown in Figure 1. The primary proton beam after striking the target will be dumped in one of the magnet beam absorbers which are placed inside the magnet apertures depending upon the tune of the train. This arrangement is necessitated primarily due to the spacial limitation of the target tube where the train is installed and raises the most serious questions about radiation damages of the magnet coil insulation and mechanical damages of the absorbers themselves due to thermal stresses caused by the beam.<sup>2</sup>

In this report we describe the general characteristics of the magnet beam absorbers and analyze thermal stress problems. We made an estimate of the structural strength against the thermal stress. Next we studied the thermal stresses at the maximum energy density area. The thermal diffusion effect was also considered. Finally, we established the safe limit of the beam intensity as far as the thermal stresses are concerned.

II. General Characteristics

The magnet beam absorbers are installed in the first seven magnets, D1, Q1, Q2, D2, Q3, Q4, and Q5. The D1 and Q1 absorbers are used only for collimation of the secondary particles and

the primary proton beam is not dumped in these absorbers. The Q2, D2, and Q4 absorbers are used as the beam dump.

All the magnets except for trim magnets and beam targetting magnets located upstream of the target are of main ring type. The bending magnets were fabricated with vacuum chambers and the absorbers fill the inside volume of the chamber. On the other hand the first five quadrupole magnets were fabricated without vacuum chambers to provide a better protection against radiation damages on the coils. The absorbers were machined to fill as much of the opening as practical. Cross section views of the D2 and Q5 absorbers are shown in Figures 2A and 2B. The absorbers were fabricated from 6061-T6 aluminum for strength and ease of machining. Each absorber has a beam aperture hole and a water cooling passage. Dimensions of the beam aperture holes were determined from the considerations of minimum useful apertures for the secondary particles and a clean beam dumping. Ideally, from a heat transfer point of view, the absorber should be one piece construction. However, the machining of the aperture holes precludes this possibility. Two piece construction with an appropriately selected split line allowed easier machining of the aperture hole and kept the cost low.

The two pieces are bolted together with the clearance holes being slots, machined parallel to the beam axis. Thus, if the heat transfer across the split line is not good, the parts are allowed to shift axially relative to each other. The cooling hole is 0.75 inches in diameter on all units. It was rifled bored with liberal tolerances. The cooling hole was positioned as close to the dump area as practical. Based on estimated energy deposition into the absorbers, the cooling flow rates vary from 2 gpm to 18 gpm at a temperatures rise of 20°C.

Figure 3 shows temperature dependences of yield strength and thermal stress<sup>3</sup> for 6061-T6 aluminum<sup>4</sup> when a massive body is heated locally to the temperature T from the ambient temperature  $T_0 \approx 25^\circ\text{C}$ . As will be discussed in the next section, the tempera-

ture rise in the beam absorber is sharply peaked particularly in the radial direction when the thermal diffusion during the beam pulse is small. Therefore, the thermal stress is purely compression stress. In the normal run, a beam pulse strikes the absorber and causes non-uniform temperature rise which is diffused and cooled down to the cooling water temperature before the next pulse arrives. This temperature cycle is repeated during every accelerator pulse and may damage the absorber from fatigue. Figure 4 shows fatigue strengths of 6061-T6 aluminum as functions of compression and tension stresses for  $10^6$ ,  $10^7$ , and  $10^8$  cycles at the room temperature. In the case of the beam absorber, the tensile stress is essentially zero. Then the strength limit for  $10^7$  cycles corresponds to the yield strength at the room temperature. Since the temperature dependence of the fatigue strength for 6061-T6 aluminum is not readily available, we assume that the fatigue strength has the same temperature dependence as the yield strength. Then, from Figure 3 the temperature rise per pulse of  $120^\circ\text{C}$  can be allowed for the run of  $10^7$  pulses provided that the absorber is cooled down to the cooling water temperature between the pulses. Since some damage at a small area of the maximum energy density can not completely destroy the absorber, the above limit is conservative.

We now make a stress analysis for the thin sections at the beam aperture corners which are structurally the weakest. The member is treated as a column with fixed ends. Using the straight line column analysis<sup>5</sup> the critical load,  $F_c$ , is given by

$$F_c = A (S - 31.2 \cdot C)$$

where A is the cross sectional area of the thin section (1" x 0.125"), S the yield stress,  $C = \sqrt{\frac{S^3}{27\pi^2 E}}$  and E the modulus of elasticity ( $E = 1.0 \times 10^7$  psi for aluminum). Then, the temperature difference,  $\Delta T$ , which corresponds to the critical load is given by

$$\Delta T = \frac{F_c}{\alpha EA} = \frac{S - 31.2C}{\alpha E}$$

where  $\alpha$  is the coefficient of expansion. For  $S \geq 20$  ksi the second term is about 10% of the first term which corresponds to the thermal stress due to the local heating in a massive body. Thus, the strength of the thin sections is about 10% weaker. However, since the thin sections are always arranged far from the maximum energy density area, any serious problems are not foreseen from the thin sections.

### III. Thermal Stresses

In the present analysis, we consider only the quasistatic thermal stress<sup>6</sup> which is caused by non-uniform energy distribution from cascade showers in the beam absorber. The dynamic thermal stress<sup>7</sup> which is very important for a very fast beam spill (<1 msec) is negligible for one-msec or longer spills and has been neglected.

Figures 5,6, and 7 show computed energy density distributions in aluminum as a function of the depth  $Z$ , of absorbers for different radial bins,  $R$ . The CASIM program by Van Ginneken was used. The incident proton energy is 400 GeV. The beam strikes an aluminum absorber directly in the case of Figure 5 and an aluminum target of about one interaction length is followed by an absorber at the distance,  $D$ , of 300 and 600 cm for Figures 6 and 7, respectively. They correspond roughly to the Q1 and Q2 dumps shown in Figure 1. The maximum energy density appears at the radius bin of 0 to 1 mm and around the depth of 60 cm for all the cases. The radial distribution of energy density is shown in Figure 6 for different depths. It is sharply peaked at  $R = 0$ . The effects of nuclear absorption and Coulomb scattering by the target can clearly be seen in Figures 5 and 7. The peak energy density decreases more than a factor of  $e (=2.72)$  at  $0 \leq R \leq 1$  mm but less at the larger radii. For the further downstream absorbers the maximum energy density becomes smaller.

The CASIM program computes the energy density for a single proton. The radial binning of 1 mm used in the analysis can roughly correspond to the energy density distribution for the beam of a 1 mm radius. Since the radial energy density distri-

bution has a sharp peak at  $R = 0$ , the beam divergence effect is significant. Figure 9 shows this effect for the three cases. Gaussian distributions with  $\sigma = 0, 1, 2$ , and 3 mm are superimposed to the radial energy density distribution. This effect becomes very important when the distance between the target and the absorber gets longer. For the Q2 absorber the beam divergence of 0.2 mrad gives 1.2 mm radial dispersion. Effects from magnetic fields of the D1 and Q1 are neglected.

We now study the thermal diffusion process in the aluminum absorber after the beam strikes it. For ease of computation we assume that the absorber is in the magnetic field free space and that there is no magnet between the target and the absorber. We also assume that the target is made of aluminum of one interaction length and the beam is radially symmetric. Then we can use the energy density distributions shown above. Since the magnetic field must diffuse charged cascade shower particles, the present estimate is conservative. The largest thermal stress should appear at the maximum energy density area. Since the Z dependence of the energy density is considerably smooth compared to the radial distribution, we consider only a region around  $Z = 60$  cm and assume an infinitely long cylinder with the radial energy density distribution in this region.

The equation of thermal diffusion<sup>3</sup> without heat source is in general given by

$$\frac{\partial u}{\partial t} = -k \nabla^2 u \quad (1)$$

where  $u$  is the temperature distribution function,  $t$  the time, and  $k$  the thermal diffusion constant which has a relation,  $k = \frac{\lambda}{c\rho} = 0.95 \text{ cm}^2/\text{sec}$  for aluminum. Here,  $\lambda$  is the thermal conductivity,  $c$  the specific heat and  $\rho$  the density. Using the radial symmetry and no Z dependence, equation (1) can be simplified to

$$\frac{\partial u(R, t)}{\partial t} = -k \left( \frac{d^2}{dR^2} + \frac{1}{R} \frac{d}{dR} \right) u(R, t) \quad (2)$$

If we assume that the absorber has an infinite heat sink at

$R = R_0$ , i.e.,  $u(R_0, t) = T_0 = 0$  where  $T_0$  is the ambient temperature and zero in the arbitrary unit. Then,  $u(R, t)$  can be given by

$$u(R, t) = \frac{2}{c^2} \sum_{j=1}^{\infty} \frac{J_0(\lambda_j R)}{[J_1(\lambda_j R_0)]^2} e^{-k\lambda_j^2 t} \int_0^{R_0} f(x) J_0(\lambda_j x) dx \quad (3)$$

where  $f(R)$  is the temperature distribution at  $t = 0$  and  $f(R) = 0$  for  $R \geq R_0$ .  $J_0(X)$  and  $J_1(X)$  are Bessel functions, and  $\lambda_i$  is the  $i$ th root of  $J_0(X)$ .

If the beam spill is short ( $\approx 1$  msec), the thermal diffusion during the spill is negligible. Then,  $F(R)$  is given by the energy density distribution. The energy density of  $1 \text{ GeV/cm}^3$  proton corresponds to the temperature rise of  $674^\circ\text{C}$  for  $10^{13}$  incident protons in aluminum. Let  $R_0 = 2$  cm and up to 40 terms summed in equation (3). Figures 10 and 11 show the radial thermal diffusion as a function of the time from the end of the 1 msec spill. The temperature at  $t = 0$  corresponds to the temperature rise for a pulse of  $10^{13}$  400 GeV protons.

For longer spill ( $> 1$  msec) the thermal diffusion during the spill must be taken into account. To calculate this effect we assume that the beam spill is uniform and can be approximated by a series of short spills of an equal intensity, spaced uniformly in time. Then, immediately after one short spill arrives at  $\tau$ , using equation (3) the thermal diffusion before the next short spill can be expressed as

$$u(R, \tau+t) = \frac{2}{c^2} \sum_{j=1}^{\infty} \frac{J_0(\lambda_j R)}{[J_1(\lambda_j R_0)]^2} e^{-k\lambda_j^2 t} \int_0^{R_0} [f(x) + u(x, \tau-0)] J_0(\lambda_j x) dx \quad (4)$$

where  $t$  is the elapsed time from  $\tau$ , and  $f(X)$  is the added temperature rise by a single short spill. Repeating this procedure we can calculate temperature distributions for longer spills. Figure 12 shows the maximum temperature rise at  $R = 0$  and  $60 \leq Z \leq 70$  cm for various spill lengths. The energy density distribution is taken from Figure 6. The number of protons per pulse

is  $10^{13}$ . The thermal diffusion effect is rather small even for the spill of 10 msec. The maximum temperature rises per pulse as a function of spill length are shown in Figure 13 for the three absorber arrangements with the beam divergence effects. The D is the distance between the target and the absorber as sketched in Figure 9. The radial energy density distribution is spread out when the D is longer and  $\sigma$  is larger. For such distributions the spill length does not strongly affect the maximum temperature.

#### IV. Conclusions

As discussed in the previous section we take the temperature rise of  $120^{\circ}\text{C}$  as the safe running criterion. Then, since it is reasonable to assume  $\sigma = 1$  mm and  $D = 600$  cm for the Q2 absorber, the safe limit of the beam intensity is  $1.3 \times 10^{13}$  protons per pulse. If the spill length is much longer than a few milliseconds, this limit can be larger. The absorbers located further downstream can also stand higher beam intensities. At present we are not planning to dump the primary beam at the Q1. If we do, however, the beam intensity must be reduced substantially as can be seen from Figure 13. For any test runs without the target the beam intensity must be kept as low as  $0.3 \times 10^{13}$  protons per pulse if  $\sigma = 0$  mm.

So far we have considered only the quasistatic thermal stress assuming that the beam absorber is cooled down to the room temperature before the beam pulse strikes it. It is, however, not clear how well the above assumption can be satisfied because a large fraction of the beam power is absorbed in the magnet core which surrounds the beam absorber. Temperatures will be monitored at various critical locations of the magnets during the run.

The D1 absorber will not be used as a beam dump, but act like a beam collimator. The D1 magnet and absorber will absorb

approximately 20% of the total beam power when the target is in place. This corresponds to 13 kW for the beam intensity of  $10^{13}$  protons per pulse with a repetition rate of 10 seconds at 400 GeV. Additional cooling will be provided by aluminum magnet cooling panels for the critical magnets.

REFERENCES

1. D.Edwards, S.Mori, and S.Pruss, 350 GeV/c Dichromatic Neutrino Target Train, TM-661, May 1976. The diagram shown in Figure 1 is the final design and slightly modified from the design shown in Figure 5 of this reference.
2. S.Velen, private communication. D.Early, J.O'Meara, K.Stanfield, and A.Weihmann, Report of the New Dichromatic Train Review Committee, October 1977.
3. S.Timoshenko, Strength of Materials, 3rd e., D.Van Nostrand Company, Inc., B.Boley and J.Weiner, Theory of Thermal Stresses, John Wiley & Sons, Inc., 1960.
4. ALCOA, Structural Handbook, 1960.
5. A.Vallance and V.Doughtie, Design of Machine Members, McGraw-Hill Book Company, Inc., 1951.
6. W.Kalbreier, W.C.Middelkoop, and P.Sievers, External Targets at the SPS, CERN Lab II/BT/74-1, February 1974.
7. P.Sievers, Elastic Stress Waves in Matter due to Rapid Heating by an Intense High-Energy Particle Beam, Lab II/BT/74-2, June 1974.
8. G.Hayashi and S.Izumi, Applied Mathematics (in Japanese), Yokendo, Inc., 1957.

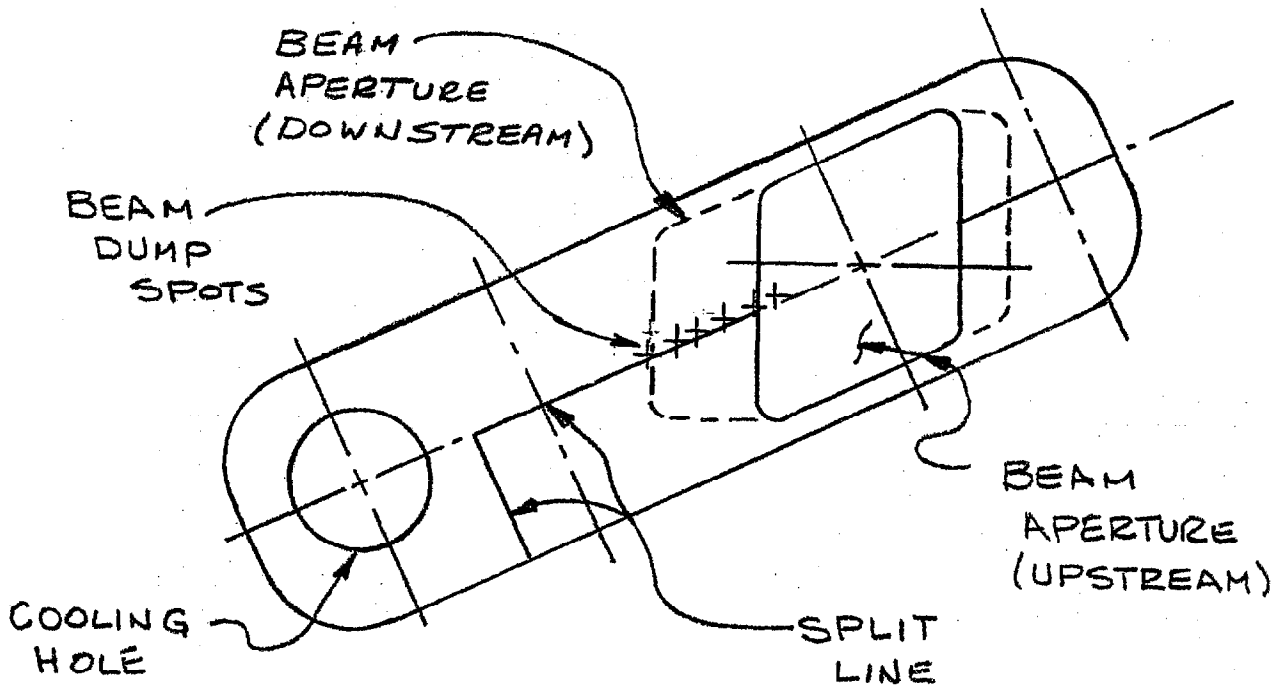
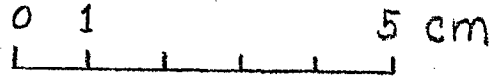
FIGURE CAPTIONS

1. Schematic diagram of the 350 GeV Dichromatic Train (N-30).
2. Cross sectional views of the magnet beam absorbers of the D2(A) and D5(B).
3. Temperature dependences of yield strengths and thermal stress for 6061-T6 aluminum.
4. Fatigue strengths as functions of tension and compression for 6061-T6 aluminum.
5. Energy density distribution for the 400 GeV incident proton in an aluminum absorber. No target is used.
6. Energy density distribution for the 400 GeV incident proton in an aluminum absorber. The target is made of aluminum of one interaction length and the distance between the target and the absorber is 300 cm.
7. Energy density distribution for the 400 GeV incident proton in an aluminum absorber. The target is made of aluminum of one interaction length and the distance between the target and the absorber is 600 cm.
8. Energy density, distribution for the 400 GeV incident proton in an aluminum absorber. No target is used.
9. Energy density distribution as a function of radius for the 400 GeV incident proton in an aluminum absorber, the beam dispersions of  $\sigma = 0, 1, 2,$  and 3 mm are superimposed.
10. Temperature rise and thermal diffusion for a 1 msec beam pulse of  $10^{13}$  400 GeV protons in an aluminum absorber. No target is used.
11. Temperature rise and thermal diffusion for a 1 msec beam pulse of  $10^{13}$  400 GeV protons in an aluminum absorber. The

Target is made of aluminum of one interaction length and the distance between the target and the absorber is 300 cm.

12. Maximum temperature rises per pulse as a function of spill length at  $R = 0$  for a beam pulse of  $10^{13}$  400 GeV protons in an aluminum absorber. The target is made of aluminum of one interaction length and the distance between the target and the absorber is 300 cm.
13. Maximum temperature rises per pulse as a function of spill length at  $R = 0$  for a beam pulse of  $10^{13}$  400 GeV protons in an aluminum absorber. The beam dispersions of  $\sigma = 0, 1$  and 2 mm are applied for three arrangements, i.e., no target case and cases with the aluminum target of one interaction length and the distances between the target and the absorbers being 300 cm and 600 cm.

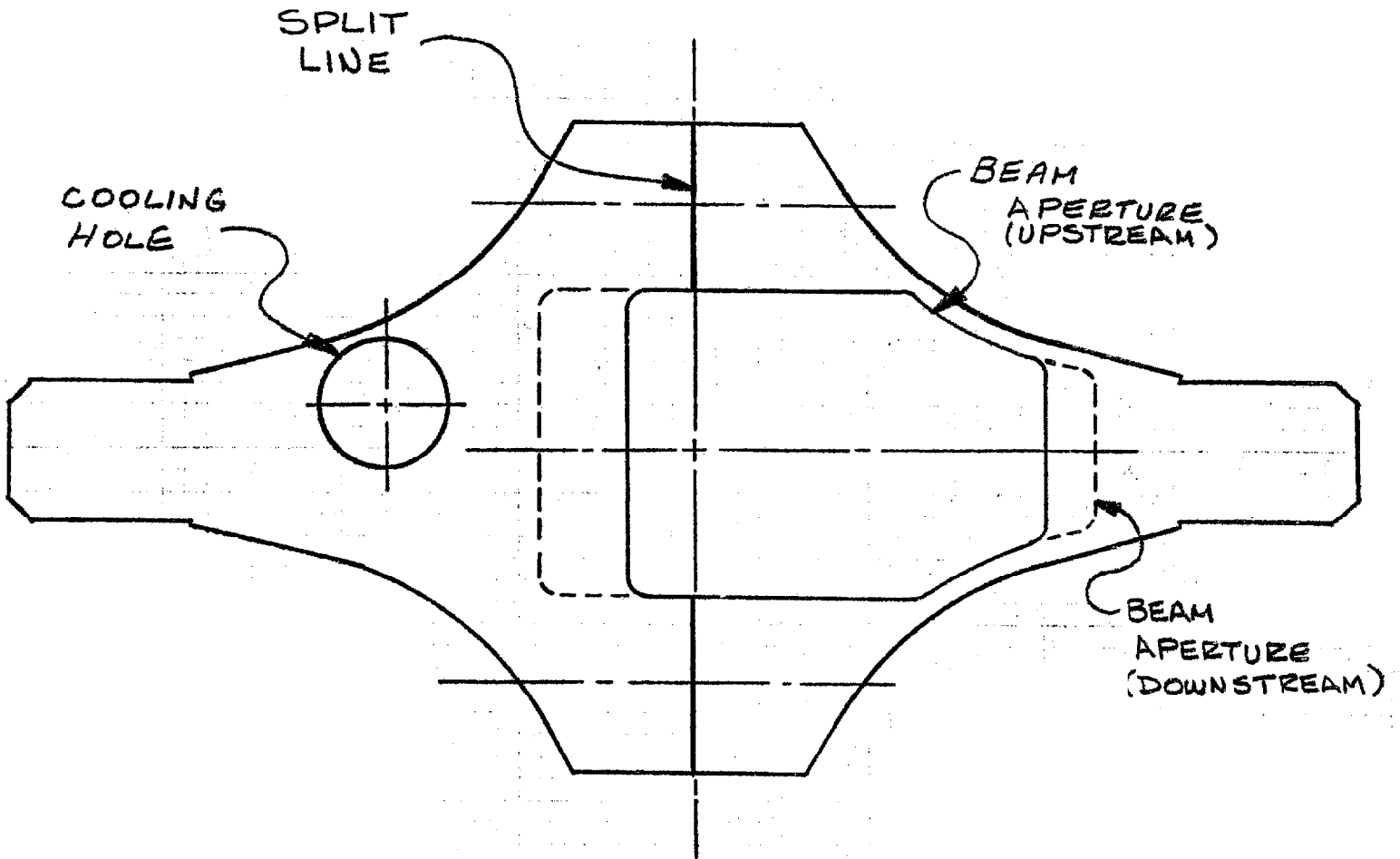




D 2 ABSORBER  
VIEW LOOKING DOWNSTREAM

Figure 2A.

0 1 5 cm



Q 5 ABSORBER  
VIEW LOOKING DOWNSTREAM

Figure 2B.

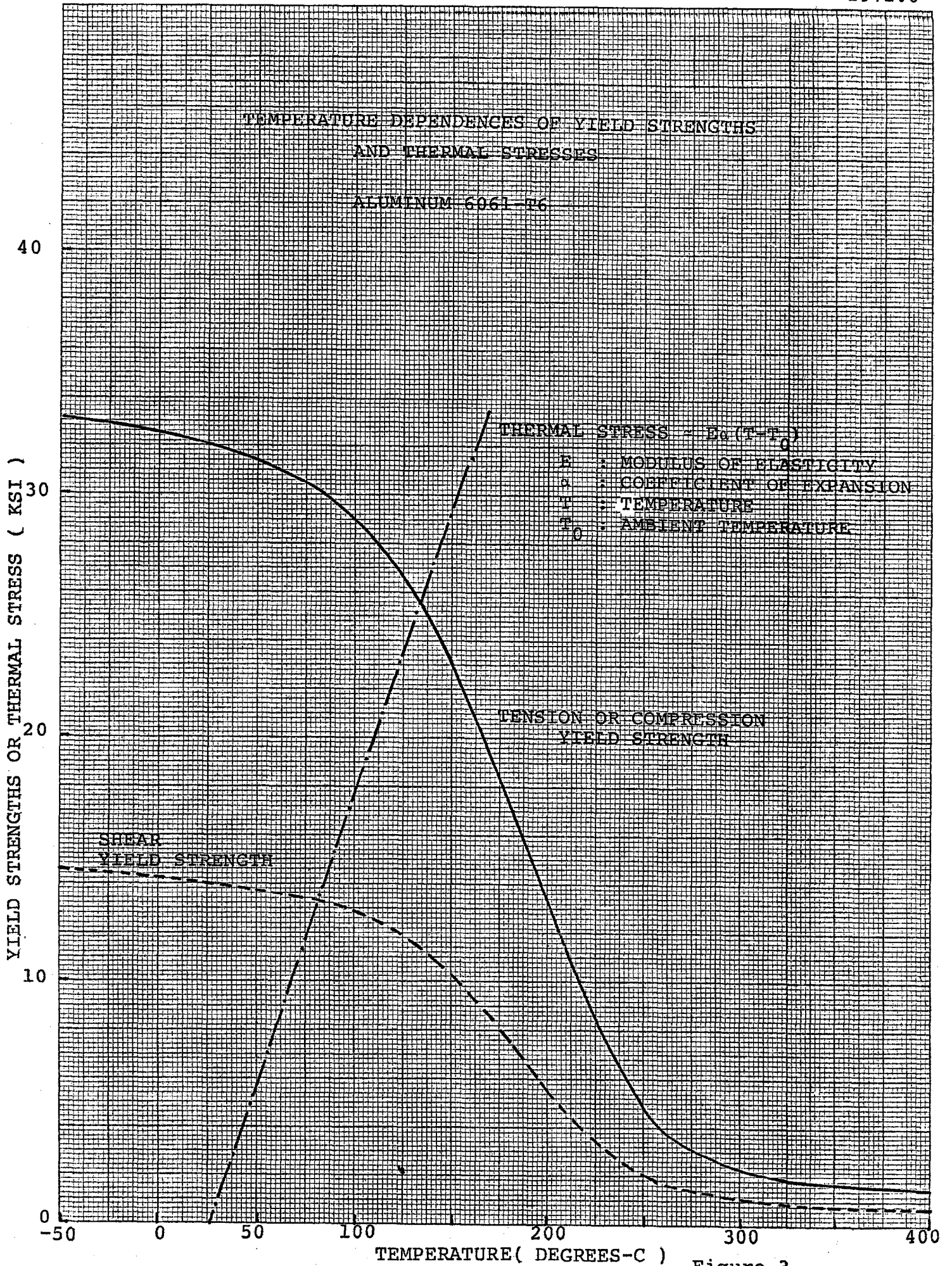


Figure 3.

FATIGUE STRENGTHS

MAXIMUM TENSION-COMPRESSION RELATION

ALUMINUM 6061-T6

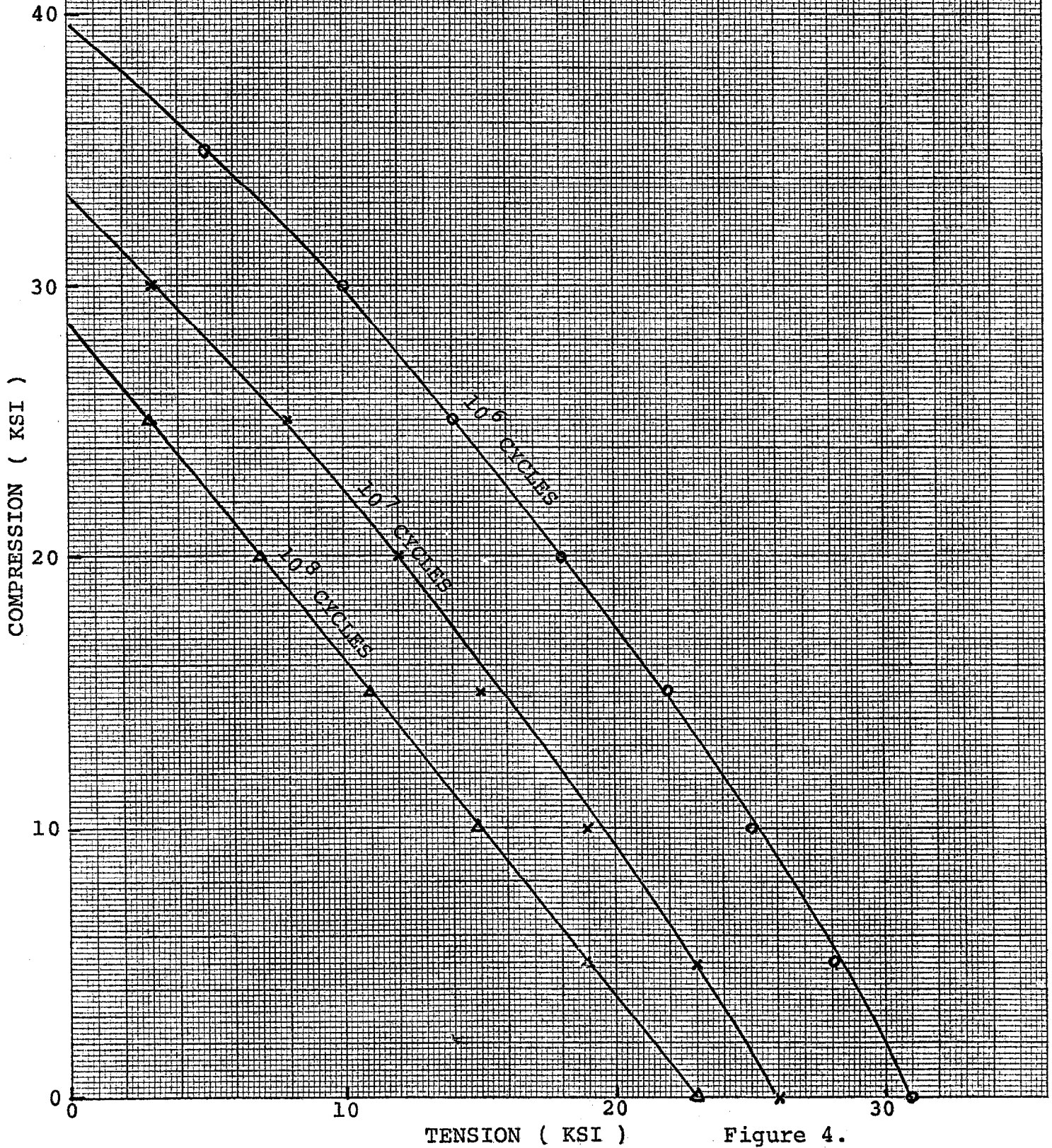


Figure 4.

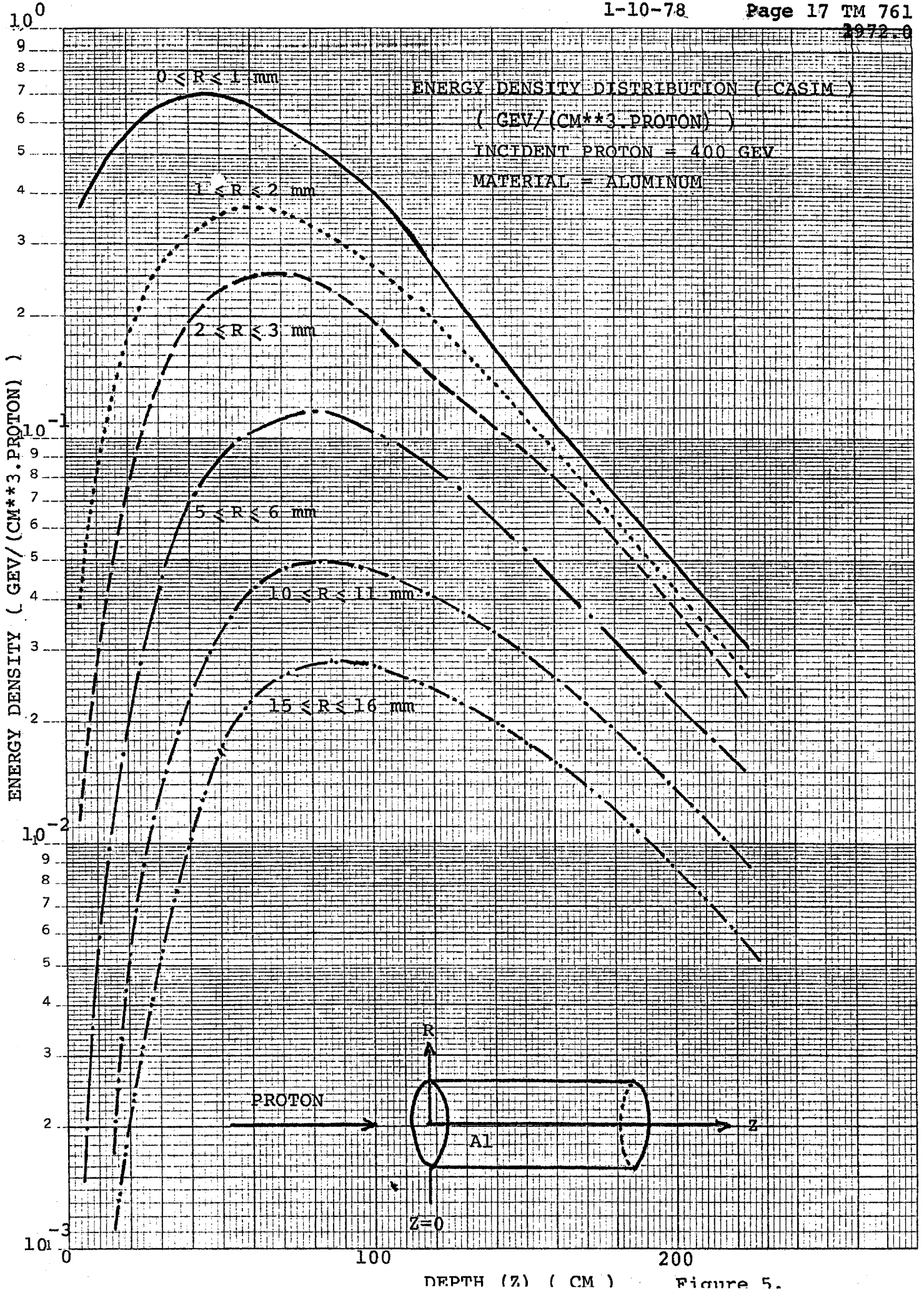


Figure 5.

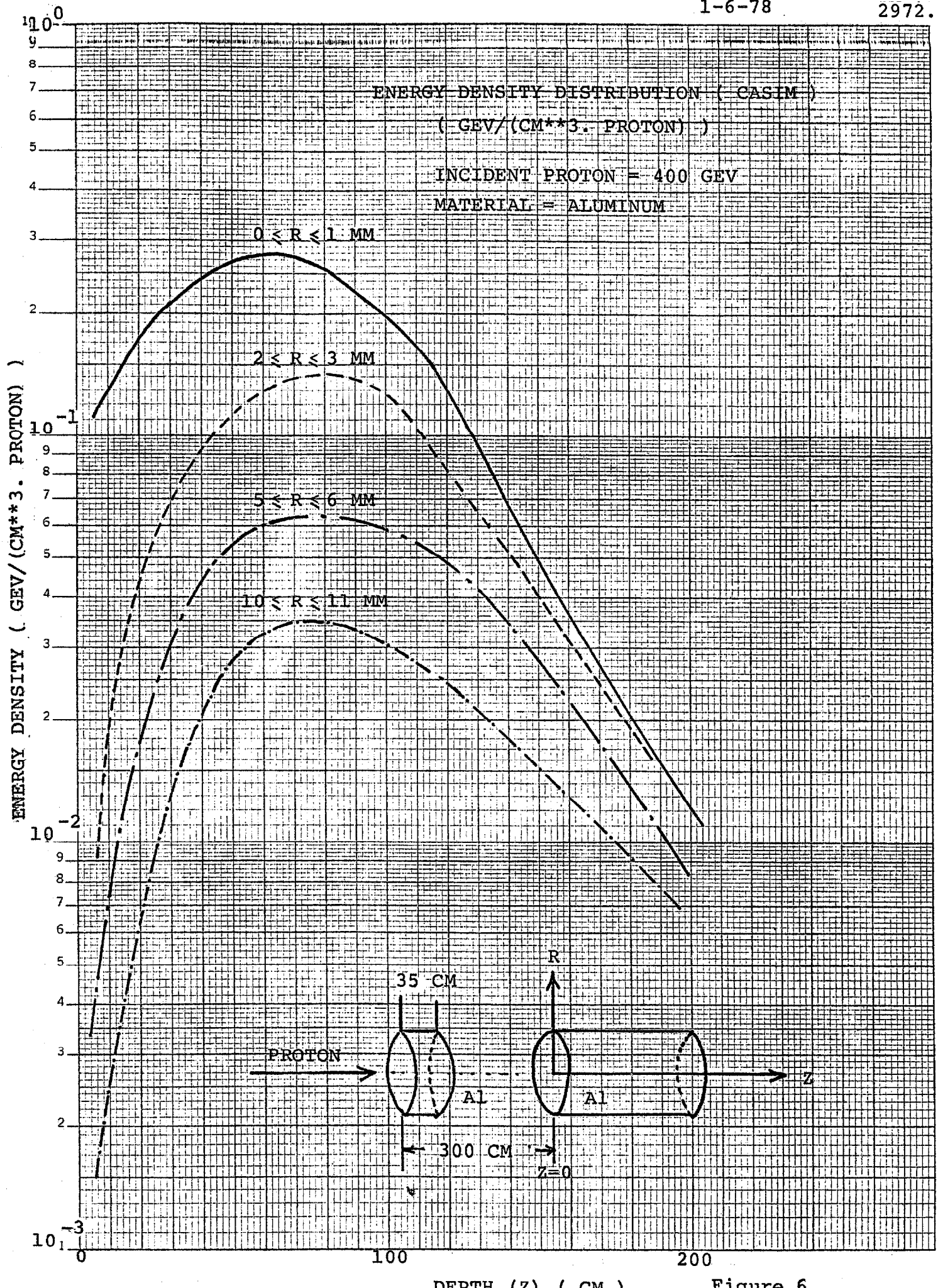


Figure 6.

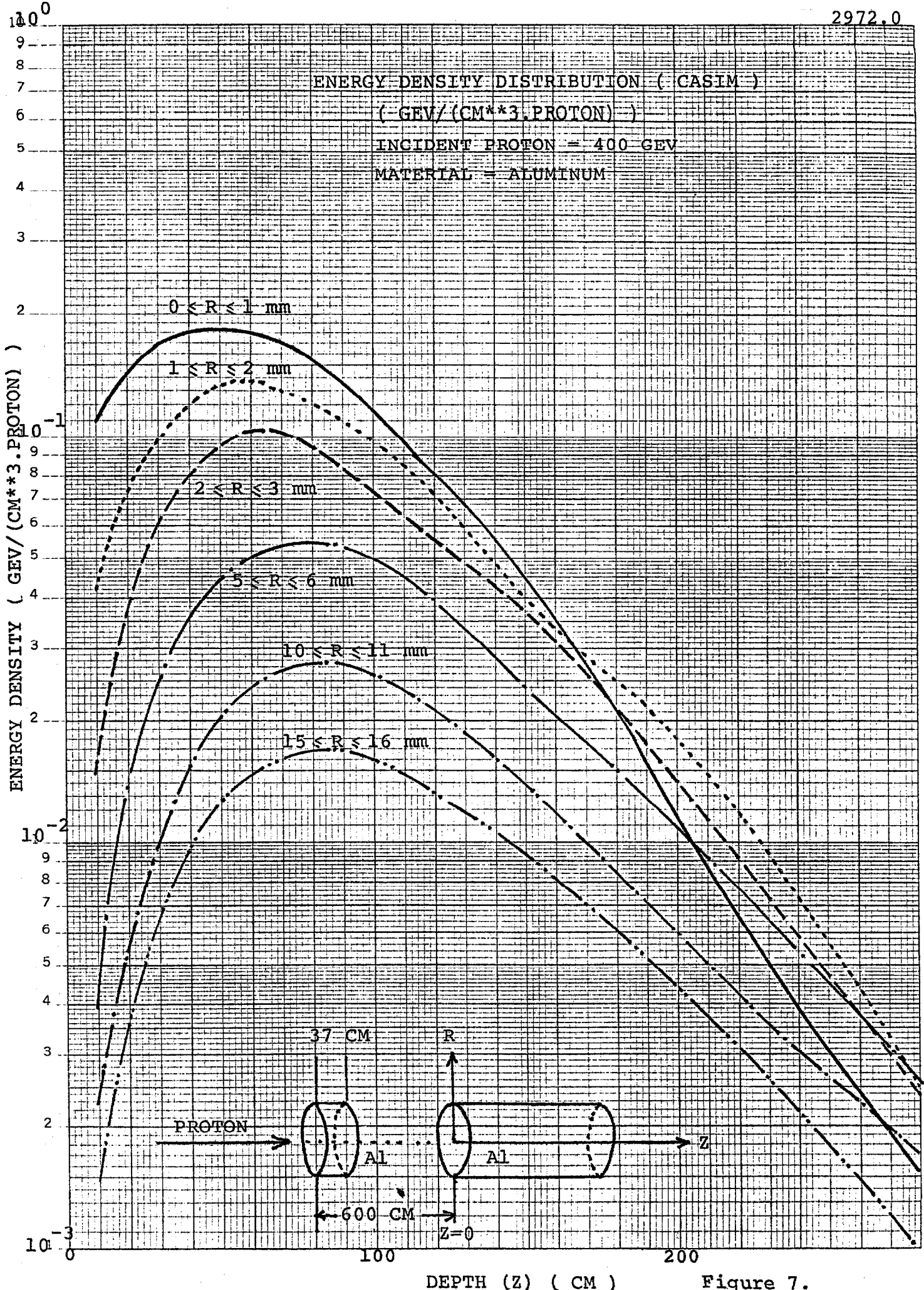


Figure 7.

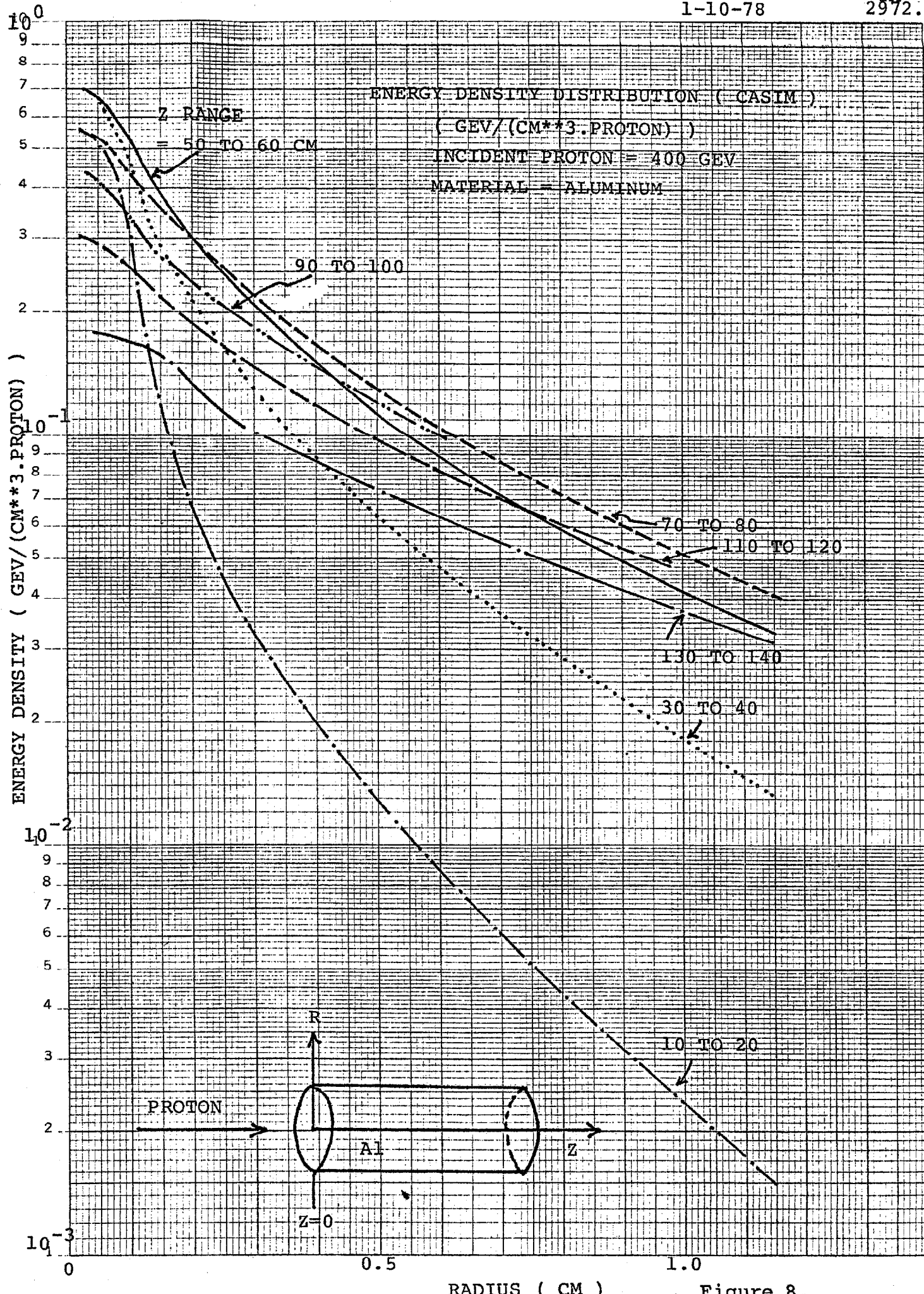


Figure 8.

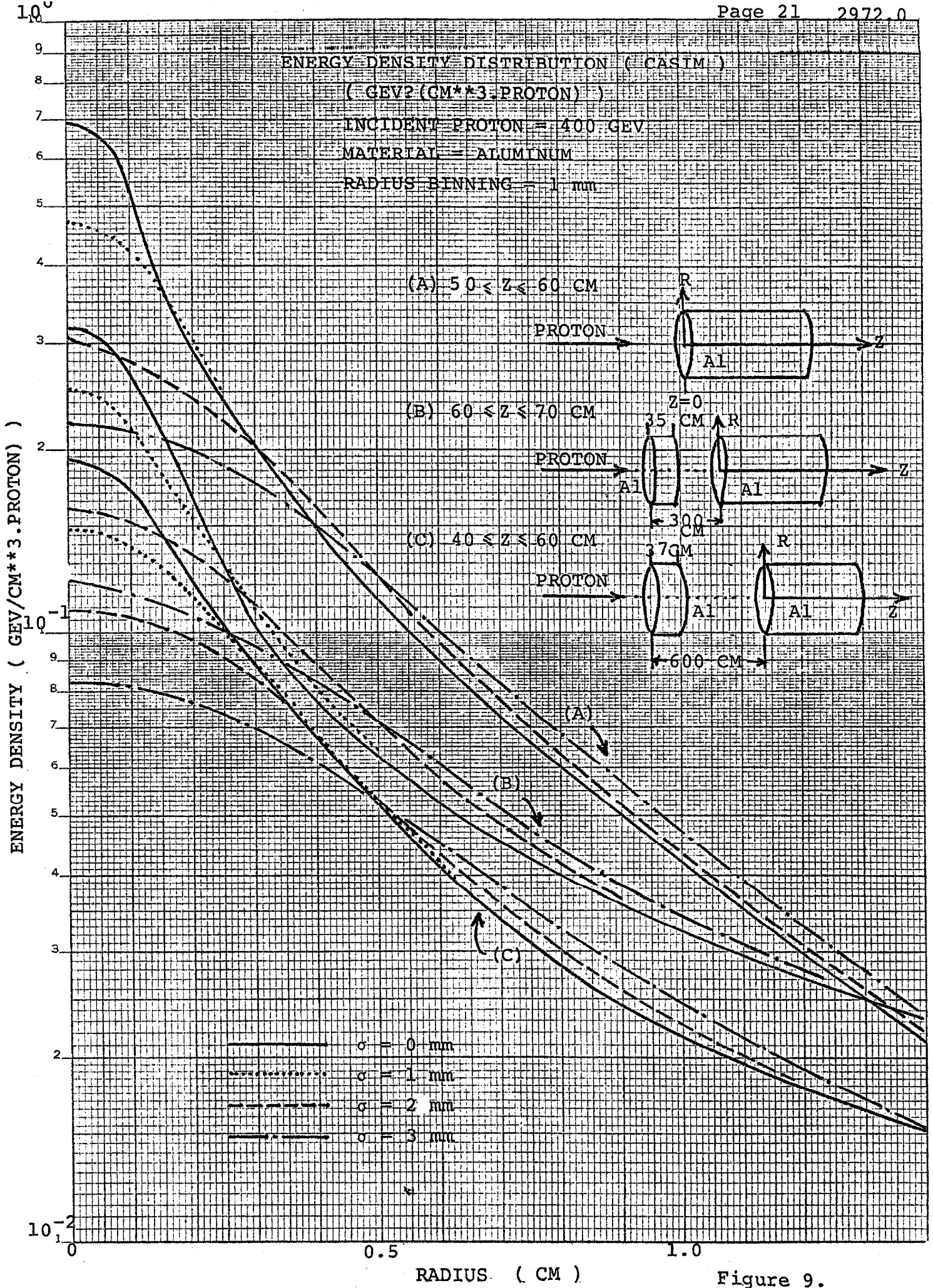


Figure 9.

### THERMAL DIFFUSION AS A FUNCTION OF TIME FROM THE END OF THE SPILL

INCIDENT PROTON = 400 GEV  
 MATERIAL = ALUMINUM  
 $10^{13}$  PROTONS PER SPILL  
 SPILL LENGTH = 1 MILLISECOND  
 $50 \leq z \leq 60$  CM

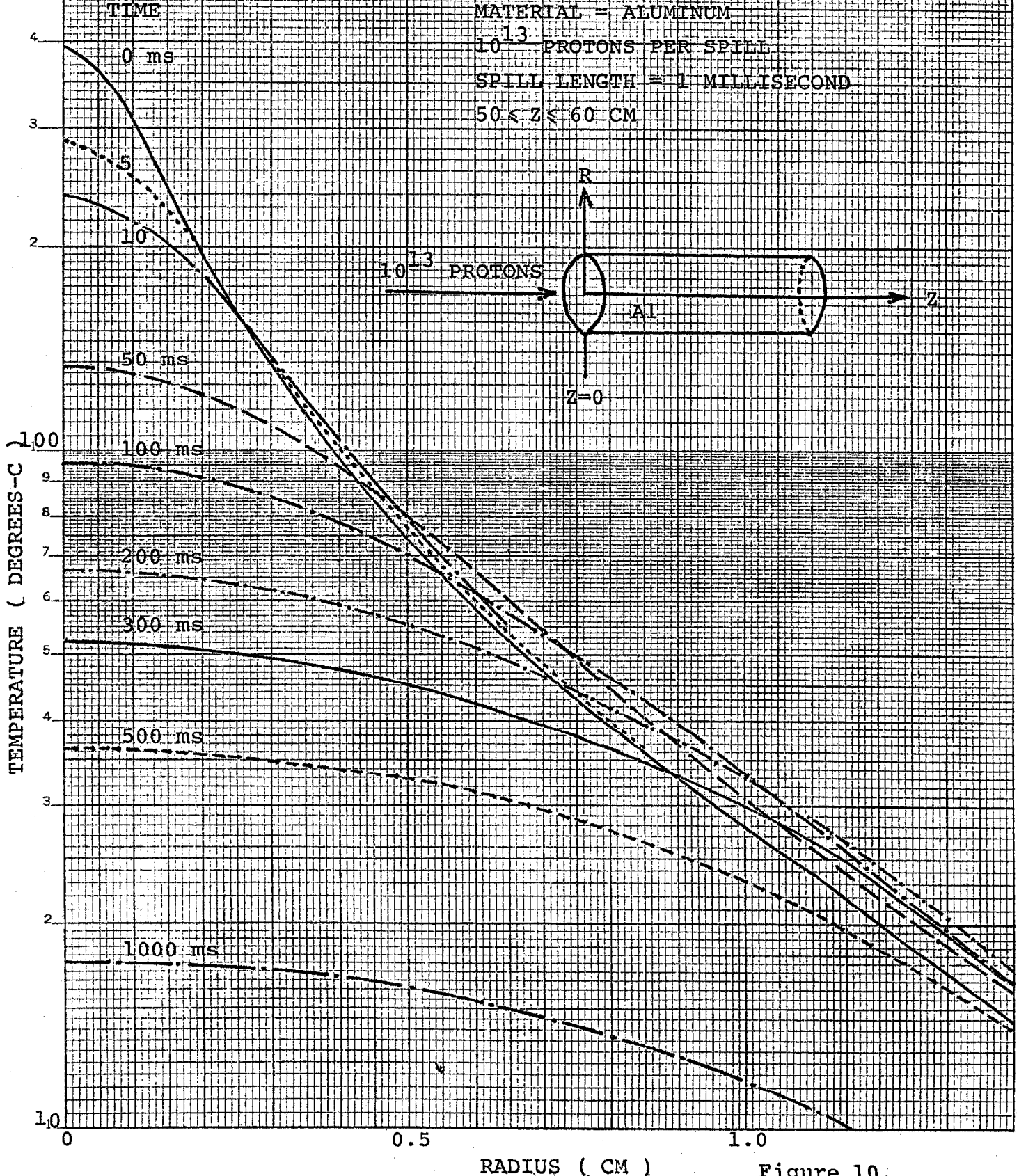


Figure 10.

THERMAL DIFFUSION AS A FUNCTION OF  
TIME FROM THE END OF THE SPILL

INCIDENT PROTONS = 400 GEV

MATERIAL = ALUMINUM

$10^{13}$  PROTONS PER SPILL

SPILL LENGTH = 1 MILLISECOND

$60 \leq z \leq 70$  CM

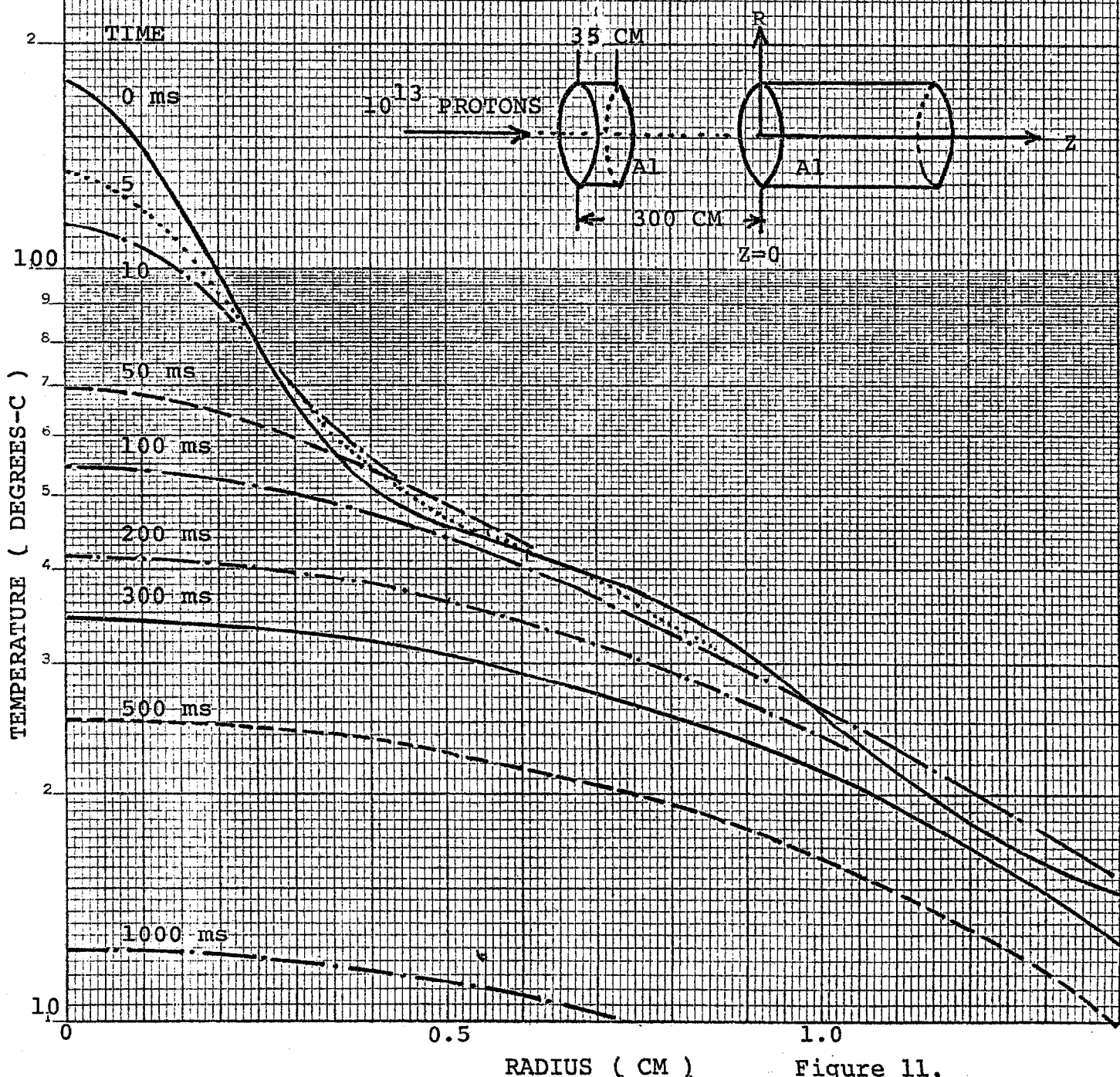


Figure 11.

1-6-78

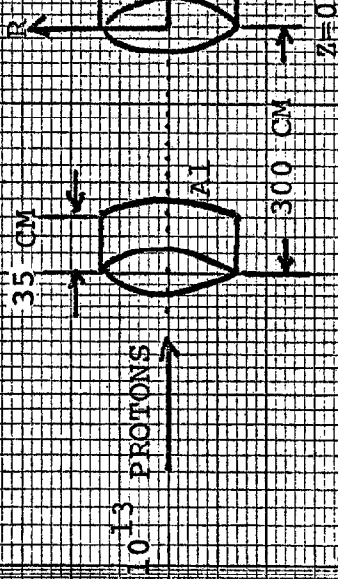
TEMPERATURE RISES PER PULSE VS SPILL LENGTH AT R = 0 MM

INCIDENT PROTON = 400 GEV

$10^{13}$  PROTONS PER PULSE

BEAM SPOT RADII = 1 MM

$60 \leq Z \leq 70$  CM



TEMPERATURE RISE ( DEGREES-C )

200

100

0

CONTOUR OF MAXIMUM TEMPERATURE RISE

SPILL = 1 ms

5 ms

10 ms

20 ms

50 ms

100 ms

1 2 3 4 5 6 7 8 9 10

10 9 8 7 6 5 4 3 2 1

100 50 20 10 5 2 1

